Laser-excited acoustic oscillations in silver and bismuth nanowires

Sergey N. Jerebtsov,[1] Alexandre A. Kolomenskii,[1] Haidong Liu,[1] Hong Zhang,[1] Zuxin Ye,[1] Zhiping Luo,[2] Wenhao Wu,[1] Gerhard G. Paulus,[1] and Hans A. Schuessler[1]

[1]*Department of Physics, Texas A&M University, College Station, Texas 77843-4242, USA*

[2]*Microscopy and Imaging Center, Texas A&M University, College Station, Texas 77843-2257, USA*

(Received 29 June 2007; published 8 November 2007)

Coherent acoustic oscillations in Bi and Ag nanowire samples were studied with a femtosecond pump-probe technique and detection of the scattered light. The observed optical and acoustic properties reflect the nanostructure of these materials. The electronic and lattice contributions to the excitation of coherent acoustic phonons are described using a two-temperature model. The excitation is performed at different laser fluences, and the high density of optically induced excitations modifies the state of the lattice. A transient state with softening of the lattice was observed in Ag nanowire samples.

DOI: 10.1103/PhysRevB.76.184301 PACS number(s): 43.35.+d, 42.25.Bs, 42.50.Md, 42.62.−b

I. INTRODUCTION

Many phenomena occurring under action of pulsed laser radiation and extensively studied in bulk materials and films,[1,2] such as electronic excitations, electron-phonon relaxation, carrier and heat diffusion, and laser generation of acoustic waves, also take place in nanostructured matter. However, they are affected by the size and the shape of the nano-objects.[3–6] The interaction of short laser pulses with nanomaterials produces coherent acoustic oscillations,[7–9] which together with microscopic studies can be used for the determination of the characteristics of light-matter interaction as well as the optical and elastic properties of nanomaterials.

Oscillations in nanostructures exhibit discrete frequency modes on the picosecond time scale due to the confinement of the acoustic vibrations. Therefore, ultrafast laser techniques are an efficient tool for their investigations. To efficiently excite a certain acoustic mode, the laser-induced transient stresses must be short enough to contain substantial spectral components at the mode frequency.[10,11] Femtosecond pump-probe techniques have been successfully applied to the studies of the elastic, thermodynamic, and optical properties as well as the acoustic modes of nanoparticles of different shapes in either solutions[12,13] or in a solid matrix.[6]

In this work, we investigated nanowires of two metals (Ag and Bi) with very different optical and electronic properties to elucidate their influence on the excitation process. While silver is characterized by a large density of free electrons, a rather large gap for interband transitions (transition edge from the *d* band of 3.9 eV), and a plasmon frequency for the bulk material corresponding to 3.8 eV,[14] bismuth is a semimetal with a relatively low density of free electrons, an overlap of the valence and conduction bands of 0.38 meV,[15] and a plasmon resonance at 14 eV.[16]

The investigations were carried out at different levels of the laser excitation with the upper limit just below the onset of irreversible structural changes in the sample. Our samples consisted of nanowires with well defined orientation, random spacing, and relatively high density. In such a system, a strong inhomogeneity of the electromagnetic field can be expected.[17] Unlike previous pump-probe experiments, which used transmitted light, the present measurements were performed by detecting the probe beam light which is quite efficiently *scattered* from the nanostructured samples.[18,19]

The high peak intensity of the laser pulses and their short duration make it possible to excite nanomaterials to a highly nonequilibrium state. We studied, in particular, the relative role of the electronic and phononic contributions to the excitation of acoustic vibrations. The periods of these vibrations, measured in pump-probe experiments, together with the information on the size of the nanowires were used to derive the elastic characteristics of the materials. In addition, acoustical responses of the Ag nanowires under high intensity laser excitation were studied.

II. EXPERIMENTAL OBSERVATION OF COHERENT ACOUSTIC OSCILLATIONS IN NANOWIRES

A. Experimental setup

For studying fast dynamic processes, a femtosecond pump-probe technique was employed. In this approach, a strong laser pulse (pump) excites lattice vibrations, which are detected by a weaker delayed laser pulse (probe). This method has a high temporal resolution which is mainly limited by the duration of the laser pulses.

The source of femtosecond pulses in our laser system is a Kerr-lens mode-locked Ti:sapphire oscillator (Kapteyn Murnane Labs, KML TS), which produces a train of pulses at a repetition rate of 87 MHz, a pulse energy of 5 nJ, and a pulse duration of about 35 fs. After amplification in a regenerative amplifier (Spectra Physics, Spitfire), the output was a train of pulses with a repetition rate of 1 kHz, a pulse energy of 0.75 mJ, and a pulse duration of about 50 fs with the central wavelength at 810 nm. The femtosecond laser pulses were characterized by both the autocorrelation technique and the frequency-resolved optical gating technique[20] based on the second harmonic generation in a nonlinear beta barium borate (BBO) crystal.

The pump and probe pulses were obtained by splitting the output of the Ti:sapphire regenerative amplifier by a 10/90 beam splitter into two parts. The 90% part was used as a source of pump pulses. Intensity of the pump beam was ad-

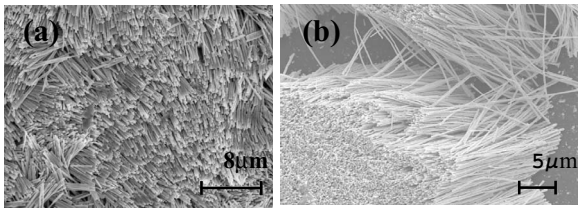

FIG. 1. SEM images of the investigated nanowire samples of large diameters ($d \approx 200$ nm): (a) Ag nanowires and (b) Bi nanowires.

justed by a neutral density filter. The pump beam was modulated at a frequency of half the repetition rate of the laser by a mechanical chopper. The 10% beam was directed onto a second harmonic generation BBO crystal and the generated blue light at 405 nm was used as the probe. The spots of the pump and probe beams with diameters of about 0.6 and 0.4 mm, respectively, were formed on the sample surface by a lens of focal length 150 mm. The light scattered from the sample surface was collected by a lens and registered by a cooled photomultiplier tube (PMT) (EMI 6255B). A blue filter (Schott, BG 12) was placed in front of the PMT to block the scattered pump light. The output of the PMT was processed with a gated integrator (SR 250) and measured by a lock-in amplifier (PAR 124). The output of the lock-in amplifier is proportional to the change induced by the pump beam in the intensity of the scattered probe light. This signal was stored in a computer.

B. Samples of nanowires

The samples of Ag and Bi nanowires used in this study were fabricated by electrochemically depositing metals into the pores of porous membranes and prepared for measurements, as described in the Appendix. The nanowires were perpendicular to the planes of the porous membranes used as templates. To reduce heating, the nanowires were studied in water. Thus, the sample with nanowires of the larger diameter $d \approx 200$ nm consisted of nanowires about 15 μm long, freestanding on a glass slide in water with a filling factor, defined as the volume fraction of the nanowires in the sample, $f \sim 0.5$. Nanowires of the smaller diameter ($d \approx 63$ nm for Ag nanowires and $d \approx 74$ nm for Bi nanowires) were electroplated into the pores of transparent polycarbonate membranes with a thickness of about 5 μm. The polycarbonate membranes were not etched away. In this case, the samples consisted of nanowires embedded in the polycarbonate membranes with a filling factor of $f \sim 0.1$, and the samples were submerged in water during the measurements. Scanning electron microscopy (SEM) micrographs of the larger diameter Ag and Bi nanowires are shown in Fig. 1.

To obtain the size distribution and structural characteristics of the nanowires, SEM micrographs and transmission electron microscopy (TEM) micrographs of the samples were taken (see the Appendix).

For the smaller diameter Ag and Bi nanowires inside a polycarbonate membrane, the extinction spectrum was measured. The light from a halogen lamp was collimated with two pinholes and the resulting beam was incident perpendicular to the surface of the membrane. The light transmitted through the membrane was detected with a spectrometer (Ocean Optics, SD 2000). The result of the measurement is presented in Fig. 2(a). For Ag, the broad resonance peak with the maximum around 530 nm can be attributed to the surface plasmon resonance in the nanowires. The transmission through the sample was about 10% at 400 nm and 50% at 800 nm.

Our samples of nanowires have significant filling factors. At these conditions their optical properties can be described by an effective medium theory.[14] The effective dielectric constant ϵ_{eff} was calculated from the Bruggemann equation,[21] which has been shown to give a good approximation for samples with imbedded nanorods[22] and nanowires[23] at high filling factors,

$$f\frac{\varepsilon_1 - \varepsilon_{eff}}{\varepsilon_1 + 2\varepsilon_{eff}} + (1-f)\frac{\varepsilon_2 - \varepsilon_{eff}}{\varepsilon_2 + 2\varepsilon_{eff}} = 0, \quad (1)$$

where ε_1 is the dielectric function of the nanowires, ε_2 is the dielectric constant of the surrounding medium, and f is the filling factor. The absorption coefficients calculated with the dielectric constant given by Eq. (1) are shown in Fig. 2(b). In the calculations the dielectric constant of the polycarbonate matrix was assumed to be constant $\varepsilon_2 = 2.6$ (Ref. 24); for Ag and Bi, the information on the dielectric function was taken from the Ref. 25. Although the calculation did not account for scattering, the general shape of the dependence is reproduced reasonably well. However, the absolute values for the transmission of light with the calculated absorption are significantly lower than the values observed experimentally (see the Discussion).

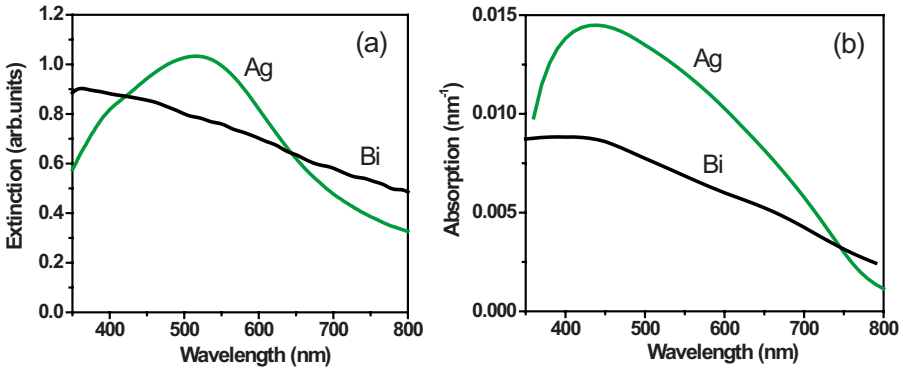

FIG. 2. (Color online) (a) Extinction spectra of the samples with small diameter Ag and Bi nanowires measured in experiment and (b) the absorption spectra calculated for the same samples (details in the text).

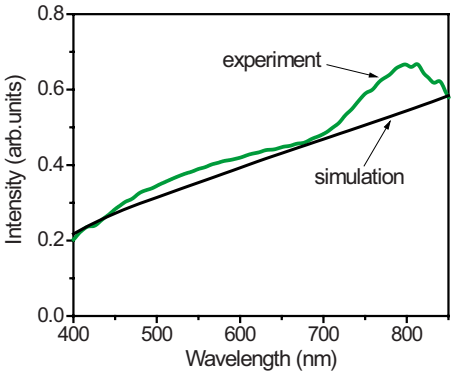

FIG. 3. (Color online) The normalized spectrum of the scattered light measured on sample with large diameter Ag nanowires and the result of a reflectance simulation based on the effective dielectric constant obtained from Eq. (1).

For the larger diameter nanowires, almost all light incident on the surface of the sample was absorbed or scattered. The optical properties of the Ag nanowires sample were characterized by a normalized spectrum for the light of the halogen lamp scattered from the sample surface and measured with the Ocean Optics spectrometer (Fig. 3).

From the dielectric constant determined with Eq. (1), the spectral dependence of the reflectivity was calculated. It qualitatively follows the spectral dependence of the scattered light observed in the experiment. The sample with the thick Bi nanowires looked gray in the scattered light showing featureless spectrum.

C. Experimental results

1. Acoustic vibrations in Bi nanowires

The acoustic response of the nanowire samples was studied. The energy of the pump pulses at the sample was set to 1 μJ for samples with the smaller diameter nanowires and to 2 μJ for samples with the larger diameter nanowires. The energy of the probe pulses was 100 nJ. The measured signals are presented in Fig. 4. In the observed signals, the initial peak, which is due to the response of the excited electronic subsystem, is followed by an oscillating signal. In the insets, the oscillating part of the signals and the fits with a damped cosine function of the form $A\exp(-t/\tau)\cos(2\pi/T+\varphi)$ are presented [see also Eq. (11) and the related discussion].

From the fits, we obtain the oscillation period $T=49$ ps and damping time $\tau=280$ ps for the sample with thinner nanowires, and $T=107$ ps and $\tau=200$ ps for the sample with thicker nanowires.

D. Acoustic vibrations of Ag nanowires at low pump excitation

For experiments on Ag nanowires, pump and probe beams of energies similar to the experiments with Bi nanowires were used: for the pump pulses, the energy was about 1 μJ for the sample with thinner and 2 μJ for the sample with thicker nanowires, and for the probe pulses, it was 100 nJ. The measured signals for the smaller and larger diameter Ag samples are presented in Fig. 5.

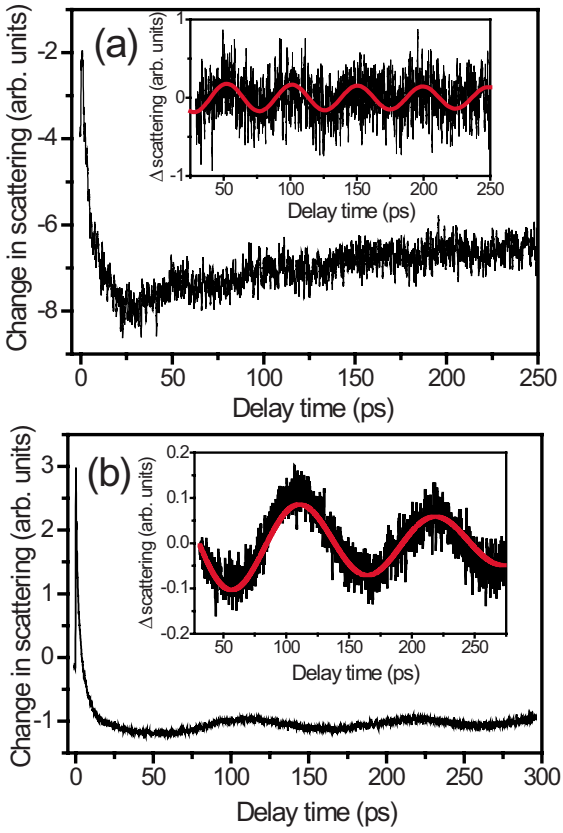

FIG. 4. (Color online) Transient signals measured from (a) a sample with thinner Bi nanowires and (b) a sample with thicker Bi nanowires. The insets show the oscillating parts of the signals fitted by a damped cosine function.

In the observed signals, the initial peak, accompanying the photoexcitation of the electronic subsystem, is followed by an oscillating signal. The fits in Fig. 5 shown as thick solid lines were done using a damped cosine function. From the fits, we obtain the oscillation period $T=28$ ps and damping time $\tau=70$ ps for the smaller diameter nanowires, and $T=71$ ps and $\tau=190$ ps for the larger diameter nanowires.

E. Acoustic oscillations of Ag nanowires at high pump excitation

The signals measured on samples with thinner and thicker nanowires are presented in Figs. 6 and 7, respectively. For each sample, the signals are the average over several measurements from the same spot on the sample. The energies of the pump pulses were set to 4 μJ for the thinner nanowires and 20 μJ for the thicker nanowires. The energy of the probe pulses was 100 nJ for both samples. The inset shows the oscillating part of the signal (upper trace) and also for reference the acoustic signal and the fit for the same sample with the low energy pump pulses (lower trace). For the high energy pump pulses, the signal shows the first oscillation with a period similar to the excitation with the low energy pulses; however, then the amplitude of the oscillations abruptly decreases and their period becomes significantly longer.

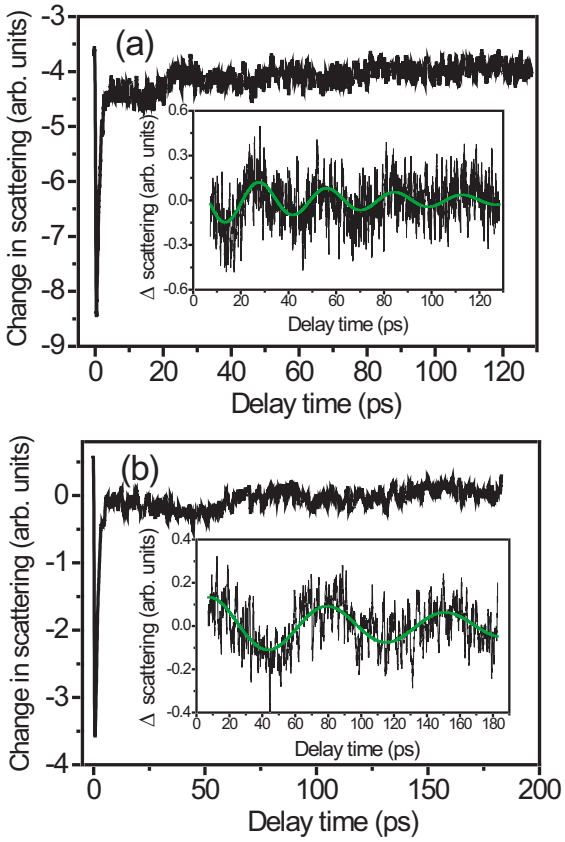

FIG. 5. (Color online) Transient signals measured (a) with thin ($d \approx 63$ nm) Ag nanowires and (b) with thick ($d \approx 200$ nm) Ag nanowires. The insets show the oscillating parts of the signals fitted by a damped cosine function.

III. THEORY

The acoustic oscillations are produced due to laser-induced variations δn_e and δn_{ph} of the electron and phonon distribution functions[2] that result in stress

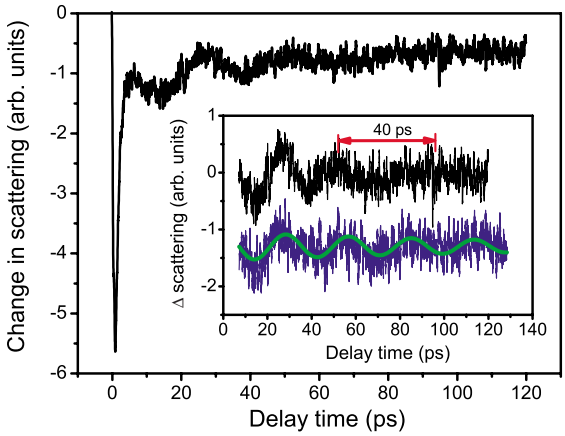

FIG. 6. (Color online) Transient signal from a sample with thinner Ag nanowires (63 nm) at high excitation level (fluence ≈ 1 mJ/cm^2). The inset shows the oscillating parts of the signals at this high fluence (upper trace) and at a lower fluence (≈ 0.3 mJ/cm^2, lower trace) for comparison.

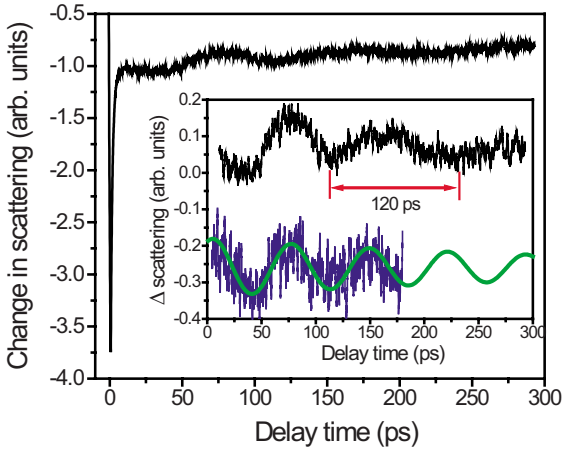

FIG. 7. (Color online) Transient signal from a sample with thicker Ag nanowires (200 nm) at high excitation level (fluence ≈ 5 mJ/cm^2). The inset shows the oscillating parts of the signals at this high fluence (upper trace) and at a somewhat lower fluence (≈ 2 mJ/cm^2, lower trace) for comparison.

$$\sigma_{ij} = \sum_{\boldsymbol{k}} \delta n_e(\boldsymbol{k}) \frac{\partial E_{\boldsymbol{k}}}{\partial u_{ij}} + \sum_{\boldsymbol{k}} \delta n_{ph}(\boldsymbol{k}) \hbar \frac{\partial \omega_{\boldsymbol{k}}}{\partial u_{ij}}, \tag{2}$$

where $E_{\boldsymbol{k}}$ is the energy of the electrons and $\omega_{\boldsymbol{k}}$ is the frequency of the phonons with wave vector $\boldsymbol{k}$. The electrons in the conduction band quickly thermalize within about 100–200 fs (Refs. 26 and 27) via electron-electron scattering, achieving a quasi-equilibrium distribution with an effective temperature of the electrons that can be much higher than the temperature of the lattice. The subsequent transfer of energy from the electrons to the lattice is often described by a two-temperature model.[28] The recombination of the carriers depends on the level of excitation,[29,30] but usually takes place on a longer time scale.

A. Two-temperature model

In the two-temperature model,[28,31] the electrons and phonons are treated as two subsystems, each characterized by its own temperature, that exchange energy via electron-phonon interactions. The dynamics of the system is described by two coupled equations:

$$C_e(T_e) \frac{dT_e}{dt} = -g(T_e - T_l) \tag{3}$$

and

$$C_l \frac{dT_l}{dt} = g(T_e - T_l) - (T_l - T_{room})/\tau_2, \tag{4}$$

where C_e, T_e and C_l, T_l are the thermal capacities and temperatures for the electrons and the lattice, respectively, and the constant g describes the electron-phonon coupling. The thermal capacity of the electrons is temperature dependent and for not very strong excitation is proportional to the electron temperature $C_e(T_e) = \gamma T_e$ and is much smaller than the thermal capacity of the lattice. In a low excitation regime,

the temperature of the lattice is much smaller than the electron temperature and the solution of Eqs. (3) and (4) can be approximated as

$$T_e - T_0 = B_1 f_1(t) \quad \text{and} \quad T_l - T_0 = \frac{g\tau_1}{C_l} B_2 f_2(t), \tag{5}$$

where $\tau_1 = g/(\gamma T_0) \ll \tau_2$, $f_1(t) = \exp(-t/\tau_1)$, and $f_2(t) = \exp(-t/\tau_2)[1-\exp(-t/\tau_1)]$. Correspondingly, there are two contributions (F_e, F_L) to the excitation of acoustic modes related to the variations in the electronic temperature and the lattice temperature given by

$$|\boldsymbol{F}_e| = |\gamma_e C_e \nabla T_e| = B_1 f_1(t)$$
$$\text{and} \quad |\boldsymbol{F}_l| = |\gamma_L C_L \nabla T_L| = B_2 f_2(t), \tag{6}$$

where γ_e and γ_l are Grüneisen constants for the electrons and for the lattice, respectively,[32] and the amplitudes B_1 and B_2 will be used for fitting later.

The temperature of the electronic subsystem decreases relatively quickly in few picosecond, which is much shorter than the period of acoustic oscillations. Therefore, the electronic contribution can be approximated by a δ function (impulsive excitation). The lattice contribution decays relatively slowly due to thermal diffusion and the exchange with the environment; consequently, it can be approximated by a step function (displacive excitation).

B. Excitation of phononic modes

First, we describe the excitation process in a system of freestanding nanowires. We consider the following problem. The laser beam is normal to the top end of a nanowire, which coincides with the $z=0$ plane, and the positive z direction is along the nanowire.

There are two major factors that lead to variations of the optical constants due to coherent acoustic oscillations in the nanowires: the oscillations of their radius and the corresponding variations of the material density. These oscillations are related mainly to standing longitudinal waves (eigenmodes), with displacements perpendicular to the long axis of the nanowires. The excitation of a longitudinal acoustic wave is described by the wave equation

$$\frac{1}{c^2}\frac{\partial^2 \boldsymbol{u}}{\partial t^2} - \Delta \boldsymbol{u} = \boldsymbol{F}_e + \boldsymbol{F}_l, \tag{7}$$

where $\boldsymbol{u}$ is the displacement and the right hand side contains contributions from the electrons $(\boldsymbol{F}_e)$ and the lattice $(\boldsymbol{F}_l)$ [see Eq. (6)]. Since the acoustic impedance of the metal $[(\rho c_l)_{(\mathrm{Ag})} \approx 3.8\times 10^7$ kg m^{-2} s^{-1}, $(\rho c_l)_{(\mathrm{Bi})} \approx 2.2\times 10^7$ kg m^{-2} s$^{-1}]$ is much larger than the impedance of the surrounding medium $[(\rho c_l)_{(\mathrm{water})} \approx 1.5\times 10^6$ kg m^{-2} s^{-1}, $(\rho c_l)_{(\mathrm{Polycarbonate})} \approx 2.7\times 10^6$ kg m^{-2} s$^{-1}]$, the free boundary conditions at the top and lateral surfaces of the nanowire can be used,

$$\left(\frac{\partial u_z}{\partial z}\right)\bigg|_{z=0} = 0 \quad \text{and} \quad \left(\frac{\partial u_r}{\partial r} + \frac{\nu}{1-\nu}\frac{u_r}{r}\right)\bigg|_{r=a} = 0. \tag{8}$$

The solution of this boundary problem can be obtained by taking into account reflection from the free boundary $z=0$ and applying a Fourier transformation over time and the x, y coordinates. For simplicity, we will consider the case of axial symmetry about the z axis and assume that the source can be factorized in the form $F(\boldsymbol{r}, z, t) = F_e + F_L = T(t)R(r)Z(z)$, with $Z(z) = \exp(-\mu z)$, where μ has the meaning of an effective absorption coefficient. Then, the radial velocity can be expressed as the sum over the eigenmodes of the nanowire,

$$u_r(r,\varphi,z,t) = \sum_{j=0}^{\infty} g_j S(z,t) J_1(\xi_j r/a)), \tag{9}$$

where

$$S(z,t) = \int_{-\infty}^{\infty} d\omega \tilde{T}(\omega)\exp(i\omega t) Q(\omega)\left(\frac{-i\mu e^{ik_{j,z}z}}{k_{j,z}} + e^{-\mu z}\right),$$

$$\tilde{T}(\omega) = (2\pi)^{-1}\int_{-\infty}^{\infty} T(t)\exp(-i\omega t),$$

$$Q(\omega) = 1/(\mu^2 + k_{j,z}^2), \quad k_{j,z} = \mathrm{sign}(\omega)\sqrt{(\omega/c)^2 - (\xi_j/a)^2}.$$

The factors $g_j \propto \int_0^\infty dr\, rR(r)J_1(\xi_j r/a)$ determine the overlap of the source distribution with the eigenmodes of the radial oscillations. The eigen numbers ξ_j are solutions of the equation

$$\xi J_0(\xi) - \frac{1-2\nu}{1-\nu} J_1(\xi) = 0, \tag{10}$$

where $J_{0,1}(x)$ are the Bessel functions of order 0 or 1, respectively, and ν is Poisson's ratio. The first three solutions for Ag ($\nu=0.37$) are $\xi_{1,2,3} \approx 2.21$, 5.44, 8.61 and for Bi ($\nu=0.33$) $\xi_{1,2,3} \approx 2.16$, 5.42, 8.59, where we take the values of Poisson's ratio for the bulk material.

The magnitude of the radial oscillations quickly decays with depth z over a distance $\sim\mu^{-1}$. The temporal dependence, determined by the function $S(z_0, t)$, contains a factor $Q(\omega)$, which for small absorption μ can strongly increase the spectral component at the resonance frequency of the radial oscillations $\omega_{r,j} = (c_l \xi_j / a)$. Note that the increase in the amplitude will be additionally limited by the damping of the oscillations due to the emission of waves in the surrounding medium, the internal friction in the material, and the viscosity of the environment. We take the damping into account by adding an exponential decay factor with a characteristic time τ, so that the temporal dependence of the signal takes the form

$$T(t) = A\exp(-t/\tau)\cos(\omega_{r,1}t + \varphi), \tag{11}$$

where the phase φ is determined by the expression

$$\varphi = \arg\left[\left(\frac{1}{\tau_2^{-1} + i\omega_{r,1}} - \frac{1}{\tau_2^{-1} + \tau_1^{-1} + i\omega_{r,1}}\right) + \frac{1}{\tau_1^{-1} + i\omega_{r,1}}\frac{B_1}{B_2}\right]. \tag{12}$$

Taking into account relations between the parameters, $\tau_1^{-1} \gg \omega_{r,1} \gg \tau_2^{-1}$, the phase can be approximated by

$$\varphi = \tan^{-1}(\omega_{r,1}\tau_1 B_1/B_2), \tag{13}$$

with an explicit dependence on the ratio of the amplitudes of the impulsive and displacive contributions.

TABLE I. The measured phases of the acoustic oscillations of the nanowire samples, the ratio of the amplitudes of the electronic and the lattice contributions (B_1/B_2), and the ratio of the effective contributions $\omega_r\tau_1(B_1/B_2)$, obtained by fitting the signal with the expressions of Eqs. (11) and (12).

	Ag (63 nm)	Ag (200 nm)	Bi (74 nm)	Bi (200 nm)
Measured phase (rad)	0.12±0.06	−0.76±0.04	−0.35±0.07	−0.15±0.01
B_1/B_2	1.9±0.2	−6.1±0.4	0.1±0.3	0.05±0.05
$\omega_{r,1}\tau_1(B_1/B_2)$	0.5±0.05	−0.6±0.04	0.036±0.13	0.008±0.008

It should be noted that at certain conditions, higher order vibrational modes can also contribute to the observed signal, although their amplitudes are expected to be substantially lower, because of the oscillating function in the integral for factors g_j. These higher modes were not observed in our experiments.

C. Numerical simulations

We performed simulations according to the described model using the following values: $\nu=0.37$ and $\tau_1=1.2$ ps for Ag nanowires and $\nu=0.33$ and $\tau_1=1.8$ ps for Bi nanowires. For each material, the characteristic time τ_1 was determined from the observed decay of the initial peak in the signals of Ag and Bi nanowires. A slight slope in the tailing parts of the observed signals in Figs. 4–7 can be attributed to the thermalization of nanowires with the surrounding medium. Consequently, it was estimated from this relatively slow relaxation process that time τ_2 exceeded 100 ps, so that the condition $\tau_2 \gg \tau_1$ was fulfilled for all the samples, and we assumed in the calculations $\tau_2=100$ ps.

The phase of the observed oscillations depends on the relative role of the electronic and lattice contributions [Eq. (12)]. We fit the phase by varying the ratio (B_1/B_2) in Eq. (12) and taking into account only the breathing mode. The obtained ratios (B_1/B_2) and $\omega_{r,1}\tau_1(B_1/B_2)$ are presented in Table I.

IV. DISCUSSION

The signals observed with Ag and Bi nanowires show certain similarities and also differences. The initial peak in the response corresponds to an increase in scattering for Bi and a transient decrease of the scattering signal for Ag, independent of the diameters of the nanowires. The dynamics of this initial peak, related to the heating and thermalization of the electron-phonon system, was thoroughly studied for nanoparticles in solutions in Ref. 33. It was demonstrated that the sign of the peak depends on the electronic temperature, and it can change depending on the wavelength relative to the spectral position of the plasmonic absorption band. With higher excitation energy, the plasmon absorption band in Ag becomes less pronounced and experiences a redshift. For the wavelength of the probe beam [405 nm, left wing of the plasmonic band, Fig. 2(a)], this leads to a reduction of the absorption and scattering cross sections. For Bi with a pump beam at 810 nm, the electrons are efficiently promoted from the valence to the conduction band, which leads to an increase of the electronic density, contributing also to the increase of the scattered signal.

The transient signals obtained from all four samples studied in the present work exhibit oscillations induced by coherent acoustic vibrations of the nanowires. The observed oscillating signals have the same initial sign for both Ag and Bi samples. These signals arise from the variations of the dielectric properties of the sample with the induced oscillations of the density and diameter of the nanowires. There are two contributions to these oscillations: one is due to electronic excitations and the other is produced by the lattice heating. The analysis of the phases of these oscillations reveals the relative role of these two contributions. From the data in Table I, we can conclude that for Bi nanowires the contribution of the electrons is relatively small for both measured samples. For the smaller diameter Ag nanowires, the obtained phase shifts are comparable to the value $\omega_r\tau_1(B_1/B_2)\approx 0.35$ obtained with Ag nanoparticles and a theoretical estimate $\omega_r\tau_1(B_1/B_2)\approx 0.42$ for bulk silver.[11] However, a negative value of the ratio B_1/B_2 was obtained for the thicker nanowires. The negative phase shift can be facilitated by several factors: an increase of the electron-phonon thermalization time (τ_1), the generation of higher harmonics, and the negative sign of the electronic contribution (F_e) in Eq. (12). Since the value of τ_1 follows from the decay of the initial peak in the transient response, it should be considered as rather well defined. The generation of the second and higher order modes, as our calculations according Eqs. (9) and (10) have shown, cannot account for the relatively large negative phase shifts. Another possible reason for this discrepancy can be the limitations of the simple linear two-temperature model of Eqs. (3)–(6) that was used, which is not strictly applicable at the high excitation levels used in experiments with thick Ag nanowires.

The observed signal depends on both the volume, where oscillations are excited, and the penetration depth of the probe beam. The excitation of the nanowires by the pump pulse is inhomogeneous, especially for the samples with larger diameter nanowires, in which the nanowire density is high. This means that other acoustic vibrations can be excited besides the pure extensional and the breathing modes. For example, an acoustic wave propagating along the nanowire at some angle can be excited. However, because of the large aspect ratio of the nanowires (length/diameter ~100 for thin and ~50 for thick nanowires), the formation of standing waves along the nanowires takes place on the nanosecond time scale. Therefore, only the radial modes can be detected within the measured range of up to ~200 ps.

TABLE II. The longitudinal sound velocities calculated for the Ag and Bi nanowire samples using experimental data and the isotropic elastic model.

	Ag (small)	Ag (large)	Bi (small)	Bi (large)
c_l (m/s)	3150	4000	2200	2750

If the intensity of the pump pulses is not very high, the oscillation has a simple sinusoidal form and can be fitted with a damped cosine function. From the obtained period of the acoustic mode and the diameter of the nanowires, it is possible to determine the elastic properties of the material. From the condition of the resonance for the fundamental breathing mode,

$$c_l = \frac{2\pi a}{\xi_1 T}, \tag{14}$$

where c_l is the longitudinal sound velocity, T is the period of the fundamental breathing mode, and ξ_1 is the first eigennumber [see Eq. (10)]. Using Eq. (14), the longitudinal sound velocities for the Ag and Bi nanowires were calculated (Table II). The longitudinal sound velocities for the polycrystalline form and for different crystallographical directions of a single crystal of Ag and Bi are presented in Table III for reference. It should be noted that the presence of a medium surrounding a nanowire changes somewhat the eigen-number and also the resonance frequency. We estimated these changes using Eq. (4) for a spherical particle in a matrix from Ref. 11. The relative changes of the resonance frequency of the breathing mode are rather small: for a Bi-polycarbonate core-matrix interface ~3%, for Bi-water ~1.4%, for Ag-polycarbonate ~0.7%, and for Ag-water ~0.2%.

The values of the sound velocities obtained for both Ag samples are different from the value for the polycrystalline material. The sound velocity calculated for the thin nanowires has a value in between the values of the sound velocities for a single crystal in the ⟨1, 0, 0⟩ and ⟨1, 1, 0⟩, directions, whereas that calculated for the large diameter nanowires is in between the sound velocities for a single crystal in the ⟨1, 1, 0⟩ and ⟨1, 1, 1⟩ directions. The acoustic properties of the nanowires depend on the structure of the material. The electron diffraction analysis of the nanowire crystal structure shows that for both samples, the nanowires consist of crystallites of a relatively large size with the length on the order of 1 μm. For a single crystal material, the value of the longitudinal sound velocity depends on the direction of propagation of the acoustic wave. The fundamental breathing mode corresponds to expansion and contraction in the radial direction, probing the crystal properties across the nanowires.

TABLE III. The longitudinal sound velocities for different crystallographic directions and for the polycrystalline form (pc) of Ag and Bi (Refs. 34–36).

Direction	⟨1, 0, 0⟩	⟨1, 1, 0⟩	⟨1, 1, 1⟩	pc
Ag, c_l (m/s)	2689	3710	4437	3650
Bi, c_l (m/s)	2540	2571	1972	2200

The longitudinal sound velocity obtained for the large diameter Bi nanowires is larger than the sound velocity for the polycrystalline bulk material and than the sound velocities of the single crystal material listed in Table III. One possible explanation is that these nanowires have fewer defects than the bulk crystal and are correspondingly stiffer.[37,38] For the small diameter Bi nanowires, the value of the sound velocity is close to that of the bulk polycrystalline material. The analysis of the nanowire structure by electron diffraction (see the Appendix) showed that, similar to the other samples, it consists of large crystallites.

The transient acoustic response of Ag nanowires at high excitation levels was studied. It was found that as pump fluence is increased above some value, the shape of the experimental signal changes. For the large diameter nanowires, this change was observed at the pump fluence of $F=5$ mJ/cm^2 (Fig. 7). At this fluence, the period of the acoustic oscillation is no longer a constant: it is smaller at an earlier time and becomes larger at longer delay times. During the first cycle, the signal looks similar to that obtained at the low pump fluence with a period close to 71 ps. At later times, the period is on the order of 120 ps. The damping also appears to have increased. It should be noted that we monitored the signals over several measurements performed on the same spot of the sample, and the signals demonstrated a similar behavior. Consequently, the effect of sample degradation during the measurement can be excluded. A possible explanation of this change in the shape of the signal is a transient softening of the material of the nanowires.

For comparison, we note that the behavior of nanoparticles under strong laser excitation has been a subject of theoretical modeling and experimental studies. In experiments with Au spheres excited with intense laser pulses, a softening of the lattice was observed, although no abrupt increase in the period of acoustic oscillation that would indicate the melting of the particles was found.[39] Molecular dynamics simulations of nanoclusters with numbers of atoms from 300 up to 1500 have also been performed.[14,40] It was found that for such small particles, there is essentially no coexistence of the two phases, whereas in larger particles, the molten and solid phases can be present in the particle at the same time. The confinement of the excited acoustic vibrations of high amplitudes within a small volume excited at high densities of deposited energy also posts a question about the possible influence of the nonlinearity on the eigenmodes.

To estimate the period of the acoustic vibrations of a nanowire in the molten phase, one can use the bulk velocity for liquid silver[41] $c_l=2810$ m/s. Assuming for the liquid $\nu=0.5$, Eqs. (10) and (14) render the period of the fundamental breathing mode of a cylinder of diameter $d=200$ nm to be $T=93$ ps. This value is somewhat smaller than the interval between the crests indicated in Fig. 7. A similar estimate for the smaller diameter Ag nanowires gives the period of the oscillation corresponding to the molten phase of about 35 ps, which is also somewhat smaller than the interval between the crests indicated in Fig. 6. Thus, the longitudinal acoustic

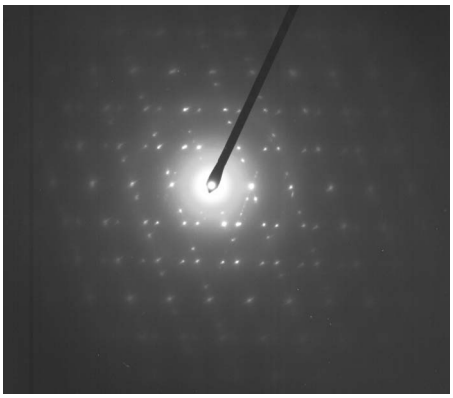

FIG. 8. Selected area electron diffraction pattern recorded from a large diameter Ag nanowire.

velocity of the nanowires in the strongly excited state approaches that of the molten phase. For understanding of this softening effect, it is important to estimate the possible heating of the nanowires.

To estimate *from above* the temperature increase in the nanowires, we assumed that the filling factor of the nanowire sample is $f=0.5$, that all the energy of the pump pulse is absorbed in the nanowires, and that the energy is deposited in the top layer of the nanowires of $l=12$ nm corresponding to the optical penetration depth of bulk silver at 810 nm. The estimate gives a temperature increase of about 3400 °C, substantially exceeding the melting temperature of bulk silver (962 °C). The provided density of the deposited energy is sufficient for melting, since the heat of fusion for silver is equivalent to heating to about 445 °C. On the other hand, if one uses the effective optical penetration depth $l(810\ \text{nm}) \approx 60$ nm, which follows from the Bruggemann formula of Eq. (1) for the composite medium, then the corresponding temperature increase is 680 °C and below the melting temperature. The observed increase of the oscillation period, on one hand, and the reproducible behavior of the sample, even after action of millions of laser pulses, on the other hand, suggest that instead of melting, a reversible transient state with softening of the lattice takes place.

A similar behavior is observed with the smaller diameter Ag nanowires. The change in the form of the experimental signal happens at a pump fluence of about $F=1\ \text{mJ/cm}^2$ (Fig. 6). Assuming that the diffusion plays only a minor role, the same density of the excitations is achieved for thin nanowires, when the combination $F/(fl)$ has the same value as for thick nanowires. This condition is fulfilled for the experimental parameters if the effective optical penetration depth l is about the same in both cases. This means that, although the sample with thin Ag nanowires transmits substantial amount of light, the major part of the energy absorption takes place closer to the tips of the nanowires. A nonuniform absorption of laser energy in resonance metal nanoparticles was predicted[42] by calculating the Poynting vector that describes the absorbed energy flux for different parts of the nanoparticle. The shapes of the spectra in Figs. 2 and 3 show that plasmon resonance effects play a role in the studied Ag nanowire samples too.

The presented estimates with the small penetration depth typical for the bulk silver provide an overly high increase of the temperature, which in reality could be substantially smaller. Indeed, the samples of thin nanowires exhibit a rather high transmission, which is not accounted for by a direct application of the Bruggemann formula of Eq. (1) rendering a penetration depth of about 100 nm for both Ag and Bi samples. A better agreement can be obtained if one takes into account the variation of the filling factor over the cross section of the sample. For a Gaussian distribution with average $f=0.1$ and the dispersion parameter of $\sigma_f=0.2$, the penetration depth increases manyfold to about 1 μm, which is already on the same order of magnitude as the experimental value of about 3 μm. However, in this approach, the spectral transmission does not vary much with wavelength in contradiction to the experimental data of Figs. 2 and 3. In addition, the homogeneous absorption along the thin nanowires cannot explain the observed softening effect. Thus, the Bruggemann formula [Eq. (1)] is not sufficient for an adequate description of the absorption, and a more sophisticated theory, taking into account the geometry of nanowires and a nonhomogeneous coupling along the length of nanowires to surface plasmon modes, is required.

TABLE IV. The diameters and the size dispersions of the samples.

	Ag (large)	Ag small	Bi large	Bi small
d (nm)	200	63	200	74
σ (nm)	20	8		8

The above arguments show that the melting of the Ag samples indeed can take place, however, the sample essentially restores its properties before the next laser pulse arrives. Thus, the formation of a transient state with a softer lattice, created by the highly excited and nonequilibrium conditions after the laser shot, is most likely. The existence of such states was demonstrated in recent studies.[43,44]

V. CONCLUSIONS

The femtosecond two-color pump-probe technique was employed for measurements of high-frequency coherent acoustic oscillations in Ag and Bi nanowire (about 70 and 200 nm diameters) samples. Unlike previous measurements, where a transmission geometry was used, the transient responses of the samples with nanowires were measured using a scattering configuration. When the intensity of the pump pulses was not very high, the oscillations had a simple sinusoidal form with attenuation. It was shown that the values of the acoustic longitudinal velocities of the samples of nanowires, obtained with the simple model of the isotropic elastic rod of a high aspect ratio, lie close to the range of the elastic constants of the bulk material. The transient acoustic response of Ag nanowires under high excitation levels was studied. It was found that at the pump fluence above certain value, the shape of the experimental signal changes. This effect can be attributed to the laser-induced transient state with substantial softening of the material.

ACKNOWLEDGMENTS

This work was supported by the Robert A. Welch Foun-

dation under Grants Nos. A1546 and A1562 and by NSF Grants Nos. DMR-0551813 and DMR-0606529. The field emission scanning electron microscopy acquisition was supported by the NSF Grant No. DBI-0116835.

APPENDIX

1. Preparation of samples

Silver and bismuth nanowires of high aspect ratio were produced by a template assisted electrochemical deposition method.[23] Commercially available filter membranes were used as the templates.

For the growth of Ag nanowires of the larger diameter ("thick" nanowires), porous anodic aluminum oxide membranes (Whatman Company, Anodisk) were employed. The main part of the membrane consists of a layer of thickness of about 55 μm with large pores of diameter of 150–200 nm (support layer) and an average porosity ~ 0.3 (from the electron micrograms after nanowire samples were produced, we determined the filling factor to be $f \sim 0.5$). This side of the membrane (the support layer) was used as the template for the growth of nanowires. To establish an electrical contact, a gold film of thickness of about 100 nm was deposited by a thermal evaporation method on the filtration side of the membrane as the cathode. The electrodeposition was performed at room temperature in a $0.05M Ag_2SO_4 + 2.3M$ KSCN solution, pH=6.0–6.5. The anode was a platinum plate of the size of 20×50 mm^2. The separation between the membrane and the anode was set to about 30 mm. A Ag/AgCl (3M NaCl) electrode was used as a reference with respect to which all potentials were measured. The overpotential voltage at the cathode, defined as $\eta = E(I) - E_0$, where $E(I)$ and E_0 are the applied and equilibrium potentials of the electrode, was set to −0.25 V. After filling the pores with nanowires, the membrane was polished from both sides with Al_2O_3 powder in order to remove the gold film and the excess of silver deposited on the surface; consequently, the thickness of the membrane with nanowires was reduced to ~ 15 μm. Next, the membrane was glued to a glass slide and the aluminum oxide template was removed by dissolving in a 5 wt % NaOH solution at room temperature for 1 h, leaving freestanding nanowires on a glass slide. The preparation method of Bi nanowires of the diameter 200 nm is similar to the above procedure.

Silver and bismuth nanowires of smaller diameter ("thin" nanowires) were produced using polycarbonate membranes (SPI, SPI-pore) of thickness of about 5 μm. The porosity of these membranes (≈ 0.1) is lower than that of the aluminum oxide membranes. The pores are randomly distributed across the membrane surface, and the average distance between the pores is about 0.4 μm. The procedure of growing the thin nanowires is similar to that for the 200 nm nanowires. After filling the pores with nanowires, the gold film and the excess of silver (or bismuth) deposited on the surface were removed.

2. Sample characterization

To obtain the size distribution of the nanowires, SEM and TEM micrographs of the samples were taken. Thick nanowires were shaken off in an ultrasonic bath and suspended in de-ionized water. To obtain the size distribution of the thin nanowires, first the polycarbonate matrix was dissolved and the nanowires were separated from the solution in a centrifuge. Then, they were washed in de-ionized water, and a drop of the solution was deposited onto a carbon film coated copper grid for TEM experiment. For accurate size measurement, all of the TEM imaging magnifications were calibrated using standards of 6H-SiC (hexagonal structure with $a = 0.3087$ nm and $c = 1.5117$ nm) lattice fringes[45] for magnifications at or above $\times 10^5$, and commercial cross-line grating replica for lower magnifications at or below $\times 8 \times 10^4$. The results of the analysis of all four samples are presented in Table IV.

To analyze the crystal structure of the material, selected area electron diffraction patterns were recorded at several locations along the nanowire length, revealing its polycrystalline nature. An example of a diffraction pattern from the large diameter Ag nanowires is shown in Fig. 8, which reveals the silver face-centered cubic structure with the presence of twins. Similar analysis was performed for the other samples.

[1] J. Hohlfeld, S.-S. Wellershoff, J. Gudde, U. Conrad, V. Jahnke, and E. Matthias, Chem. Phys. **251**, 237 (2000).
[2] C. Thomsen, H. T. Grahn, H. J. Maris, and J. Tauc, Phys. Rev. B **34**, 4129 (1986).
[3] A. P. Alivisatos, Science **271**, 933 (1996).
[4] S. Tarucha, D. G. Austing, T. Honda, R. J. van der Hage, and L. P. Kouwenhoven, Phys. Rev. Lett. **77**, 3613 (1996).
[5] S. Link and M. A. El-Sayed, Int. Rev. Phys. Chem. **19** (3), 409 (2000).
[6] M. Perner, S. Gresillon, J. März, G. von Plessen, J. Feldmann, J. Porstendorfer, K.-J. Berg, and G. Berg, Phys. Rev. Lett. **85**, 792 (2000).
[7] N. D. Fatti, C. Voisin, F. Chevy, F. Vallee, and C. Flytzanis, J. Chem. Phys. **110**, 11484 (1999).
[8] J. Hodak, A. Henglein, and G. Hartland, J. Chem. Phys. **111**, 8613 (1999).
[9] M. Nisoli, S. De Silvestri, A. Cavalleri, A. M. Malvezzi, A. Stella, G. Lanzani, P. Cheyssac, and R. Kofman, Phys. Rev. B **55**, R13424 (1997).
[10] Y.-X. Yan and K. A. Nelson, J. Chem. Phys. **87**, 6240 (1987).
[11] C. Voisin, N. Del Fatti, D. Christofilos, and F. Vallee, Appl. Surf. Sci. **164**, 131 (2000).
[12] M. Hu, H. Petrova, X. Wang, and G. V. Hartland, J. Phys. Chem. B **109**, 14426 (2005).

[13] M. Hu, X. Wang, G. V. Hartland, P. Mulvaney, J. P. Juste, and J. E. Sader, J. Am. Chem. Soc. **125**, 14925 (2003).
[14] U. Kleibig and M. Vollmer, *Optical Properties of Metal Clusters* (Springer, Heidelberg, 1995).
[15] M. S. Dresselhous, *The Physics of Semimetals and Narrow-band Semiconductors*, Proceedings of the Conference on the Physics of Semimetals and Narrow-gap Semiconductors (Pergamon, New York, 1971), pp. 1–32.
[16] C. Wehenkel and B. Gauth, Solid State Commun. **15**, 555 (1974).
[17] W. D. Bragg, V. P. Safonov, W. Kim, K. Banerjee, M. R. Young, J. G. Zhu, Z. C. Ying, R. L. Armstrong, and V. M. Shalaev, J. Microsc. **194**, 574 (1999).
[18] V. A. Sterligov, P. Cheyssac, W. Blau, and M. Kroll, Opt. Commun. **226**, 125 (2003).
[19] E. Eremina, Y. Eremin, and T. Wriedt, Opt. Commun. **273**, 278 (2007); X. D. Li, H. S. Hao, C. J. Murphy, and K. K. Caswell, Nano Lett. **3**, 1495 (2003).
[20] R. Trebino, K. W. DeLong, D. N. Fittinghoff, J. N. Sweetser, M. A. Krumbugel, B. A. Richman, and D. J. Kane, Rev. Sci. Instrum. **68**, 3277 (1997).
[21] D. A. G. Bruggemann, Ann. Phys. **24**, 636 (1935).
[22] A. K. Sarychev, R. C. McPhedran, and V. M. Shalaev, Phys. Rev. B **62**, 8531 (2000).
[23] G. Riveros, S. Green, A. Cortes, H. Gómez, R. E. Marotti, and E. A. Dalchiele, Nanotechnology **17**, 561 (2006).
[24] S. E. Caudill and W. T. Grubbs, J. Appl. Polym. Sci. **100**, 65 (2006).
[25] *CRC Handbook of Chemistry and Physics: A Ready-Reference Book of Chemical and Physical Data*, 65th ed., edited by R. C. Weast (CRC, Boca Raton, 1985).
[26] H. Inouye and K. Tanaka, Phys. Rev. B **57**, 11334 (1998).
[27] B. Rethfeld, A. Kaiser, M. Vicanek, and G. Simon, Phys. Rev. B **65**, 214303 (2002).
[28] S. I. Anisimov, B. L. Kapeliovich, and T. L. Perel'man, Sov. Phys. JETP **39**, 375 (1974).
[29] P. Tangney and S. Fahy, Phys. Rev. B **65**, 054302 (2002).
[30] M. Hase, M. Kitajima, S. Nakashima, and K. Mizoguchi, Phys. Rev. Lett. **93**, 109702 (2004).
[31] G. V. Hartland, J. Chem. Phys. **116**, 8048 (2002).
[32] G. Tas and H. J. Maris, Phys. Rev. B **49**, 15046 (1994).
[33] J. H. Hodak, I. Martini, and G. V. Hartland, J. Phys. Chem. B **102**, 6958 (1998).
[34] Y. Eckstein, A. Lawson, and D. Reneker, J. Appl. Phys. **31**, 1534 (1960).
[35] R. Bacon and C. Smith, Acta Metall. **4**, 337 (1956).
[36] J. Neighbours and G. Alers, Phys. Rev. **111**, 707 (1958).
[37] A. Krishnan, E. Dujardin, T. W. Ebbesen, P. N. Yianilos, and M. M. J. Treacy, Phys. Rev. B **58**, 14013 (1998).
[38] E. Wong, P. Sheehan, and C. Lieber, Science **277**, 1971 (1997).
[39] G. Hartland and M. Hu, J. Phys. Chem. B **107**, 7472 (2003).
[40] L. J. Lewis, P. Jensen, and J. Barrat, Phys. Rev. B **56**, 2248 (1997).
[41] T. Iida and R. Guthrie, *The Physical Properties of Liquid Metal* (Oxford University Press, New York, 1988).
[42] Z. B. Wang, B. S. Luk'yanchuk, M. H. Hong, Y. Lin, and T. C. Chong, Phys. Rev. B **70**, 035418 (2004).
[43] C. Guo, G. Rodriguez, A. Lobad, and A. Taylor, Phys. Rev. Lett. **84**, 4493 (2000).
[44] C. Guo and A. J. Taylor, Phys. Rev. B **62**, R11921 (2000).
[45] Z. P. Luo, Acta Mater. **54**, 47 (2006).